Mon. Not. R. Astron. Soc. **295,** 921–932 (1998)

# Dynamical studies of cluster pairs in the Magellanic Clouds

M. R. de Oliveira, H. Dottori and E. Bica

*Instituto de Fisica – UFRGS, Caixa Postal 15051, CEP 91501-970 Porto Alegre, RS, Brazil*

Accepted 1997 December 1. Received 1997 September 5; in original form 1997 May 28

**ABSTRACT**

We performed *N*-body simulations of star cluster encounters with Hernquist's TREECODE in a CRAY YMP-2E computer under different initial conditions (relative positions and velocities, cluster sizes, masses and concentration degrees). The total number of particles per simulation ranged from 1024 to 20480. These models are compared with a series of isodensity maps of cluster pairs in the Magellanic Clouds. Evidence is found that during the interactions, transient morphological effects such as an expanded halo, isophotal deformation and isophotal twisting can occur as a result of tidal effects and dynamical friction. The simulations also show that different outcomes are possible depending on the initial parameters: (i) long-standing changes of concentration degree can occur after the collision; (ii) one member can disaggregate; or (iii) the pair can coalesce into a single cluster with a distinct structure compared with the original ones. These simulations can reproduce a wide range of morphological structures in observed cluster pairs.

**Key words:** celestial mechanics, stellar dynamics – Magellanic Clouds – galaxies: star clusters.

## 1 INTRODUCTION

In recent years, the possible existence of physical star cluster pairs in the Magellanic Clouds has been extensively investigated (Bhatia & Matzidimitriou 1988; Bhatia & MacGillivray 1988; Bica, Clariá & Dottori 1992; Rodrigues et al. 1994, hereafter RRSDB; Bica & Schmitt 1995). The realization of the existence of such pairs is fundamental not only for a better understanding of the formation and evolution of star clusters themselves, but for the Magellanic Clouds as a whole.

In the last decade, *N*-body simulations of stellar system encounters have been the main tool with which to investigate the dynamical processes that can occur in such interactions, such as mergers and tidal disruption. Many of the first simulations worked with equal-mass encounters (White 1978; Lin & Tremaine 1983; Barnes 1988). Different-mass encounters have been carried out by Dekel, Lecar & Shaham (1980), Aguilar & White (1985) and Rao, Ramamani & Alladin (1987). Encounters of stellar system pairs, in which the number of particles in each pair member is very different, were performed by Barnes & Hut (1986, 1989) and RRSDB. Those studies indicate that tidal disruption and mergers are two important processes in the dynamical evolution of a binary stellar system. The merger time of two comparable-mass clusters is shorter than the disruption time. On the other hand, a massive primary is likely to cause disruption of the satellite and, in this case, the disruption time could be shorter than that of the merger.

The effects of tidal forces are not merely peripheral. The overall structure of the clusters is also affected. The fractional increase in the total internal energy of a cluster provides a good measure of the change in its structure (Alladin 1965).

In this work we analyse the morphologies of selected cluster pairs in the Magellanic Clouds and compare them with those obtained from numerical simulations of star cluster encounters. We also measure the fractional changes in total energy and total mass of the clusters during the simulations. As a significant number of Magellanic Cloud pairs involve clusters of different sizes, we have simulated encounters with clusters of different masses in most cases. In these encounters we have taken the relative velocity and distance of the closest approach (pericentre distance) as free parameters.

In Section 2 we describe the method and the initial conditions employed in the present simulations. In Section 3 we describe the Magellanic Cloud cluster pair images and the procedure for deriving the isodensity maps. The numerical results and comparison of models and real pairs are provided and discussed in Section 4. In Section 5 we give the main conclusions.

## 2 THE METHOD AND THE INITIAL CONDITIONS

### 2.1 The method

To calculate the force between two particles in the $N$-body simulations we used the softened Keplerian potential, given by

$$\phi(r)=\frac{-Gm_i m_j}{(r^2+\varepsilon^2)^{1/2}}, \quad (1)$$

where $G$ is the gravitational constant and $m_i$ and $m_j$ are the masses of the particles; $\varepsilon$ is known as the softening parameter (Hernquist 1987), introduced to avoid divergence when close encounters between two stars occur. This parameter also smooths fluctuations in the potential, reducing the effects of relaxation. We use a system of dimensionless units in which $G=1$. In the present models, the number of particles is comparable to the number of stars in a real cluster.

We performed the simulations using TREECODE (Hernquist 1987) in the CRAY YMP-2E computer of Centro Nacional de Supercomputação of the Universidade Federal do Rio Grande do Sul (CESUP-UFRGS).

### 2.2 The initial conditions

King (1966) provided theoretical profiles that describe well the light distribution in globular clusters. In the present models, the stellar clusters are represented by a density distribution that follows a Plummer polytrope (Aarseth, Hénon & Wielen 1974). This density profile is computationally simpler to deal with and is comparable to a classical King profile (Fig. 1). In this figure, a Plummer density distribution for a model with 4096 particles (solid line) is compared with a King profile with a concentration $c=0.70$ (dashed line), showing a good agreement. Cluster models were generated for 16384, 4096 and 512 equal-mass stars, corresponding to total masses of $10^5$, $10^4$ and $10^3$ $M_\odot$, respectively. The cut-off radii of the Plummer clusters are 20, 15 and 8 parsecs, respectively. These cut-off radii are of the order of diameters found in cluster pairs in the Magellanic Clouds (Bhatia et al. 1991). We generated two different concentration degrees for the 512-particle cluster, one with half-mass radius half of the cut-off radius and another with half-mass radius a quarter of the cut-off radius (Table 1). The models have null angular momentum. Each cluster was allowed to evolve by itself for two relaxation times to give a well-mixed, dynamically stable system. These relaxation times ranged from $10^7$ yr for the 512-particle models to $10^8$ yr for the model with 16483 particles. During this time they conserved their density profile and total energy (Figs 2 and 3), which ensures that any structure appearing in the encounters is the result of the cluster–cluster interaction. The interaction models are characterized by a pericentre distance $p$ (distance of closest approach) and the initial relative velocity $V_i$. These initial velocities are comparable to the observed random velocities in the Large Magellanic Cloud (LMC) disc (Freeman, Illingworth & Oemler 1983). The initial conditions ($t=0$) are: (i) the large cluster (in the case of equal-mass clusters, the more concentrated one) is located at coordinates $(x,y)=(0,0)$; (ii) the small cluster lies at a distance $r_0=5\times r_t$ (where $r_t$ is the tidal radius). Beyond this distance the tital effects are negligible. The initial relative velocity at this distance was obtained from the two-body formulae. The

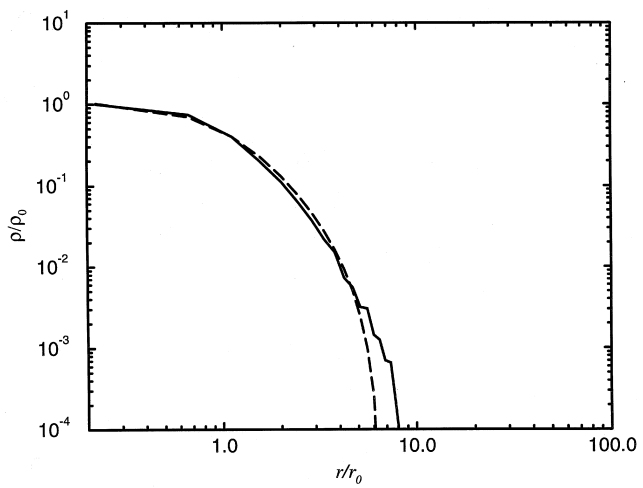


**Figure 1.** Behaviour of a Plummer density profile (solid line) and a King profile with a concentration $c=0.70$ (dashed line) for a model with 4096 particles.

**Table 1.** Input parameters for the simulations. $N_{part}$ is the number of particles of the cluster; $M_T$ is the cluster total mass; $R_h$ is the half-mass radius; $R_{max}$ is the maximum radius of the cluster; $V_{md}$ is the mean velocity of the particles (modulus); $\varepsilon$ is the softening parameter.

| Model | $N_{part}$ | $M_T$ ($M_\odot$) | $R_h$ (Pc) | $R_{max}$ (Pc) | $V_{md}$ (Km/s) | $\epsilon$ |
|---|---|---|---|---|---|---|
| A | 16384 | $10^5$ | 4.94 | 20.0 | 3.53 | 0.30 |
| B | 4096 | $10^4$ | 3.72 | 15.0 | 1.94 | 0.47 |
| C | 512 | $10^3$ | 2.00 | 8.0 | 0.83 | 0.50 |
| D | 512 | $10^3$ | 4.00 | 8.0 | 0.62 | 0.50 |

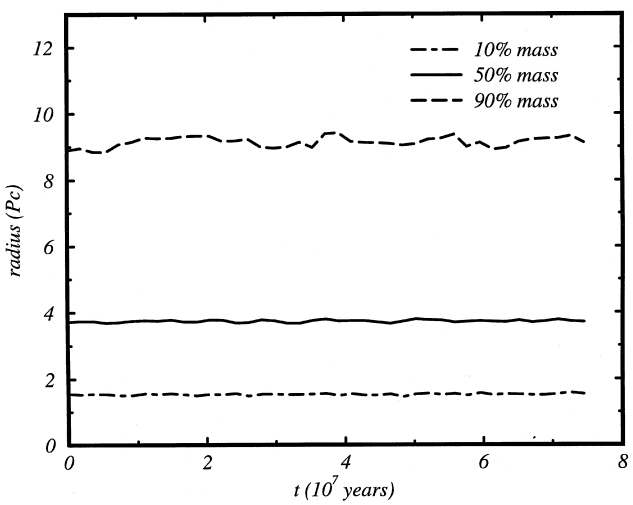


**Figure 2.** Behaviour of the radii containing 10, 50 and 90 per cent of the particles, as a function of time, for the model with 4096 particles. The time-stationary nature of the distribution is preserved by the TREECODE.

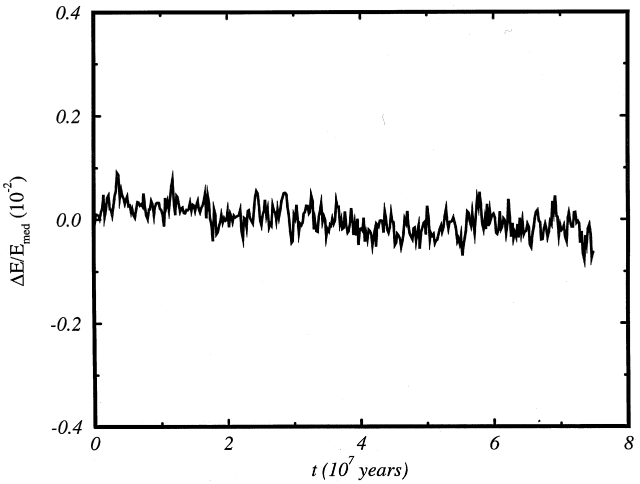


**Figure 3.** Total energy change as a function of time for the model with 4096 particles.

positions and velocities of the particles during the encounters were computed in the centre-of-mass frame of the entire system. At various times, the essential data containing the positions and velocities of all the particles were stored for later analysis. The computation was stopped when disruption of the cluster occurred or, in the case of open orbits, when the relative separation of the clusters reached the distance $d > 2r_0$.

We illustrate in Fig. 4 the time evolution of an elliptic orbit encounter involving two clusters with 4096 and 512 particles respectively (model E9BD10). Notice the evolution of the smaller cluster into a bow-like, loose, disrupted system.

## 3 ISODENSITIES OF SMC AND LMC CLUSTER PAIRS

In a recent revision of star cluster catalogues in the Small Magellanic Cloud (SMC) and LMC, Bica & Schmitt (1995) and Bica, Schmitt & Dutra (private communication), using Sky Survey ESO/SERC *R* and *J* films, checked previous pairs (e.g. Bhatia et al. 1991) and identified some new ones. We have selected pairs with morphologies resembling those of the present models (Section 4). Bhatia & Hatzidimitriou's (1988) criterion for pairs is a projected centre-to-centre separation of less than 18.7 pc. We increased this limit to 37.4 pc in order to include some clusters with possible evidence of interaction caused by a close past approach. The pair NGC 294/B 67 + BS 63 is an example that requires this new limit, since its centre-to-centre separation is $\simeq$32 pc. Distance moduli of 18.9 and 18.5 mag, respectively, for the SMC and LMC (Westerlund 1990) are adopted throughout this paper.

The images of this selection of pairs were obtained from the Digitized Sky Survey (DSS). The plates are from the SERC Southern Sky Survey and include IIIa-*J* (3600-s), *V*-band medium (1200-s) and *V*-band short (300-s) exposures. The PDS pixel values correspond to photographic density measures from the original plates, and are not calibrated.

The digitized images were treated with the IRAF package at the Instituto de Física – UFRGS, applying a 2D Gaussian filter to smooth out individual stars and creating isodensity maps. We illustrate in Fig. 5 a series of LMC pairs spanning a wide variety of morphologies. It is possible to see structures linking some pairs (BRHT 47b/BRHT 47a, NGC 2140/BM 160 and NGC 1994/anonymous companion), which may be interpreted as a sign of interaction. It is also possible to see isophotal twisting in one pair (NGC 2140/BM 160) and a common isophotal envelope in three other pairs (C9/SL 747, NGC 1836/BRHT 4b and SL 629/anonymous companion), which may again be evidence of interaction between these cluster pairs. It is possible to associate these morphologies with some of the evolutionary stages seen in the elliptical orbit encounter E9BD10 (Fig. 4). For example, the pair SL 629/anonymous companion could be associated with the stage of model E9BD10 at $t = 33.0$ Myr. On the other hand, similar morphologies may occur in the epoch of cluster formation. Evidence of this is the pair SL114/anonymous companion (Fig. 6), which has an age ($\approx$5 Myr) for one component (see Table 2) that is exceedingly small compared with similar morphology indicated by the simulation (33.0 Myr). In SL 114/companion the morphology must date from the formation epoch, rather than a late dynamical interaction. Isodensity maps of the entire sample of pairs in the Magellanic Clouds will be presented and discussed elsewhere.

The catalogue designations of the objects appearing in the present study are: BM (Bhatia & MacGillivray 1989), BRHT (Bhatia et al. 1991), BS (Bica & Schmitt 1995), B (Brück 1976), C (Hodge 1975), HS (Hodge & Sexton 1966), L (Lindsay 1958) and SL (Shapley & Lindsay 1963). Some anonymous clusters are also included.

In Table 2 we show the pairs in the Magellanic Clouds with available SWB types (Bica et al. 1996). Most of these clusters have ages comparable to or larger than the relaxation times of the models ($10^7$–$10^8$ yr; Section 2.2).

## 4 DISCUSSION

We considered models in which the less massive cluster (perturbed) is allowed to move in hyperbolic, parabolic or elliptic orbits around the more massive one (perturber). In the hyperbolic models, the perturbed cluster is assumed to move in an orbit of eccentricity $e = 5$, whereas in the elliptic case $e = 0.6$, 0.7, 0.9. The values of the pericentre and the eccentricity are meaningful only if the clusters are assumed to be point masses moving in Keplerian orbits. However, soft potential orbits are not conical and our use of these definitions is meaningful only to a good approximation, but not strictly (White 1978).

The collision parameters of the simulations are given in Table 3. The model designation (column 1 of Table 3) contains information on the encounter conditions. H, P and E refer to hyperbolic, parabolic and eliptic orbit encounters, respectively; the number following the letter E is related to the orbital eccentricity (column 5 of Table 3); A, B, C and D refer to the model type (Table 1); the last number is the pericentre of the orbit (column 6 of Table 3).

From the analysis of the time evolution of each model as illustrated in Fig. 4 for E9BD10, it is possible to infer that tidal damage occurs after the perturbed cluster has passed the closest approach point. The trend to form bridges is observed mainly in the models with elliptic orbits and low-

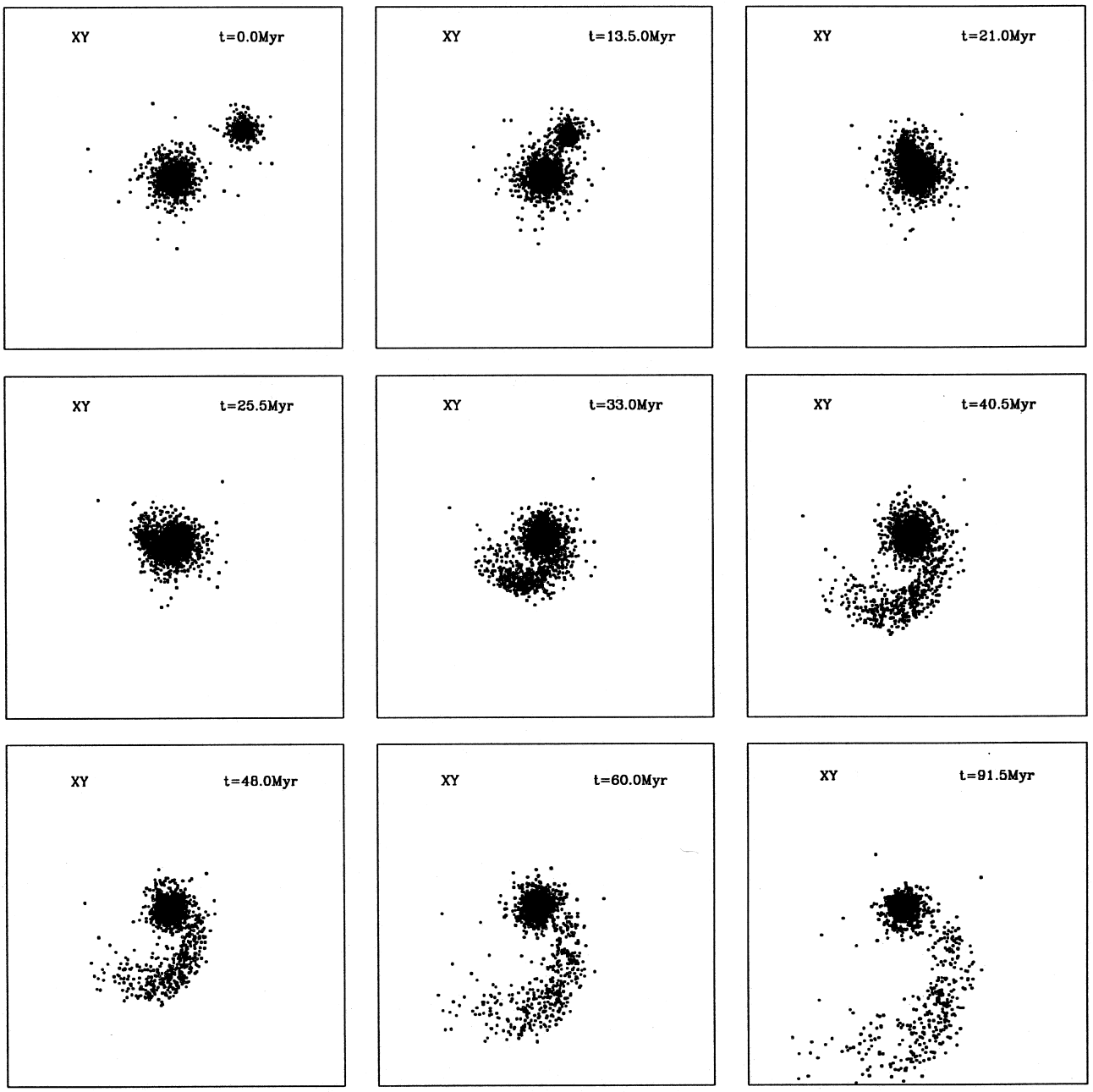


**Figure 4.** Time evolution of an encounter (model E9BD10) projected in the *XY* plane.

velocity parabolic orbits ($V < 5$ km s$^{-1}$), just after the cluster has passed the pericentre point, and survives for a long time. The central regions become more compact as a result of the encounter. In the fast hyperbolic encounters, the deformations of the perturbed cluster occur mostly in a direction perpendicular to its trajectory. Total disruption occurs in the E and P models, where the pericentre $p$ is of the order of the perturbed cluster radius $R_h$.

### 4.1 Mass loss

The mass loss of the perturbed cluster for the various models is shown in Fig. 7. Here $\Delta M = M_0 - M_f$, where $M_f$ is the mass of the final bound system. The percentage of mass loss is almost 100 per cent for the E and some P models, with the subsequent disruption and/or merger of the perturbed cluster. In the H models the mass loss is negligible, but increases as the distance of closest approach is decreased.

### 4.2 Energy change

The energy change of the cluster during an encounter is a measure of the damage it suffers. We plot the fractional change in the energy of the perturbed system $\Delta U/|U|$ as a function of time in Fig. 8. Here $\Delta U = U_f - U_0$ where $U_f$ is the final energy of the bound system and $U_0$ is the unperturbed initial energy of the cluster. In all models, most of

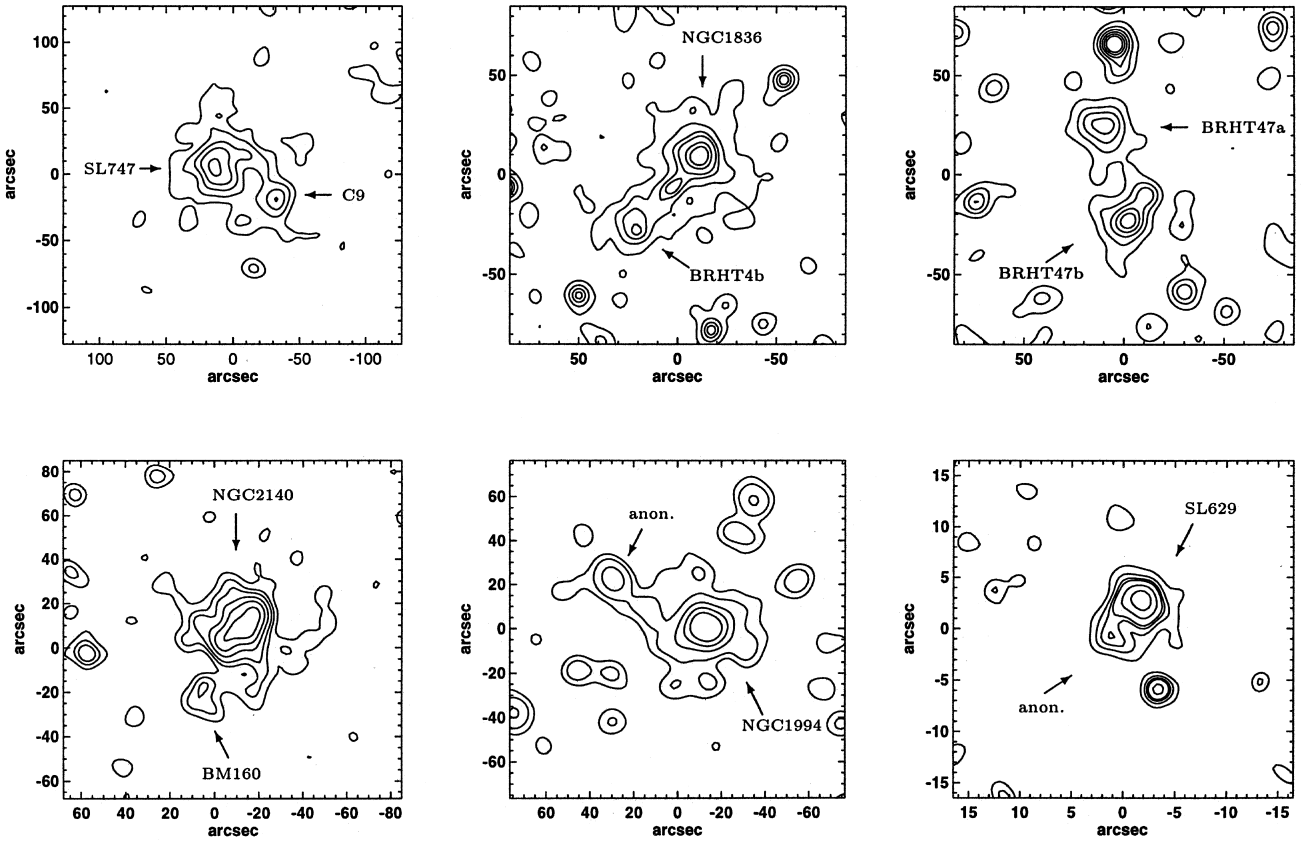


**Figure 5.** Isodensity maps of some observed cluster pairs with evidence of interaction.

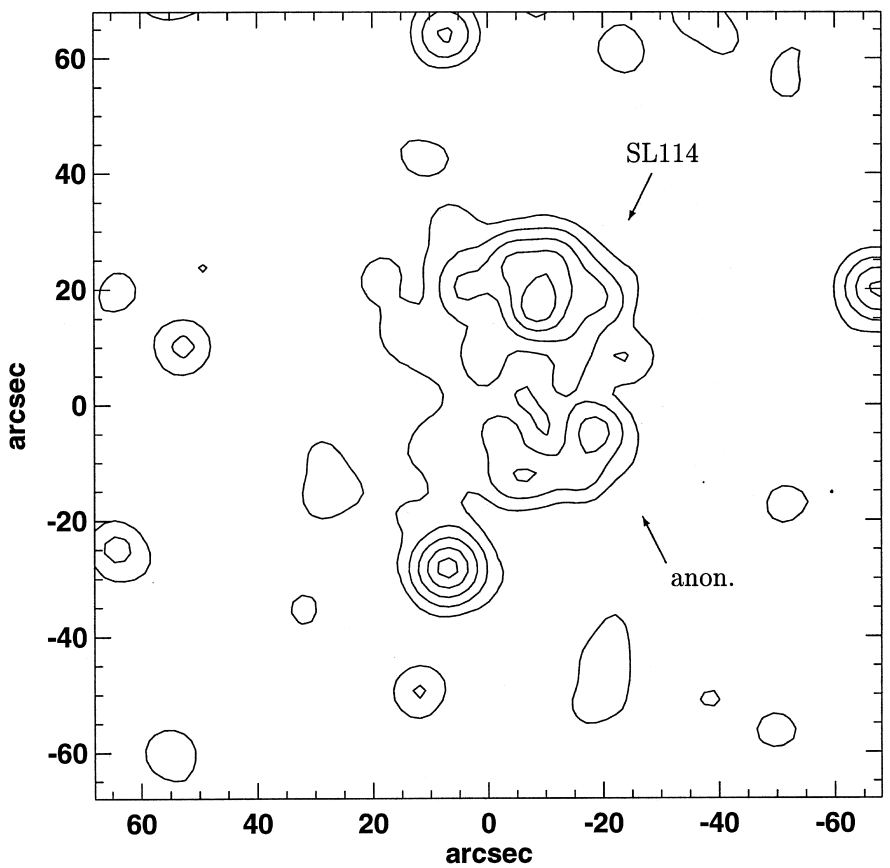


**Figure 6.** Same as Fig. 5, for a pair too young compared with the interaction time. The morphology must date from the formation epoch.

**Table 2.** Ages for members of cluster pairs in the present sample. Columns: (1) cluster identification; (2) observed visual magnitude, (3) SWB type; (4) age.

| Names | $V$ | $SWB$ type | Age (Myr) |
|---|---|---|---|
| SL114 | 11.46 | 0 | 5 |
| NGC1836 | 12.22 | III | 120 |
| NGC1994 | 9.78 | I | 20 |
| HS319 | 12.50 | IVA | 300 |
| SL747 | 13.02 | IVA | 300 |
| NGC2136 | 10.54 | III | 120 |
| NGC2137 | 12.66 | II | 50 |
| NGC2140 | 12.44 | II | 50 |
| NGC294=L47[a] | 12.26 | IVA | 300 |

[a]SWB type deduced from *UBV* colours in Alcaino (1978).

the change in the energy occurs after the perturber crosses the pericentre. In the models H and P20 the energy remains nearly constant after that, provided that disruption does not take place. In most E and P models the energy of the perturbed cluster continues to increase, which is a sign of disruption.

Disruption occurs if $\Delta U/|U| > 2$, as indicated earlier by Miller (1986). This is nearly equivalent to $\rho_h/\rho_R < 4$ (Namboodiri & Kochhar 1990) where $\rho_h$ is the mean density of the perturber cluster calculated at $R_h$, and $\rho_R$ is the density of the perturber cluster within a sphere of radius equal to the pericentre (Roche density). The condition $\Delta U/|U| > 2$ for disruption agrees relatively well with our models, except for the model E7CD5, where we have disruption of the perturbed cluster for $\Delta U/|U| \simeq 1.5$, and for the models E7BC10 and E6BC10 where, although we have almost 40 per cent mass loss, we inferred visually that until the end of our simulation there was no disruption of the perturbed cluster. The reason for this is the fact that in these last two models the criterion $\rho_h/\rho_R < 4$ was not respected. From this we conclude that in an encounter disruption occurs only for

$$p \leq 2R_h \left(\frac{M}{m}\right)^{1/3}, \quad (2)$$

where $M$ is the mass of the perturber cluster and $m$ is the mass of the perturbed cluster.

Using the ratio $M/m = 10$ for our models, we have

$$p \leq 4.3\, R_h. \quad (3)$$

### 4.3 Radial mass distribution

A quantitative estimate can be made for the shape of a system of particles from the values of $\langle|X|\rangle$, $\langle|Y|\rangle$ and $\langle|Z|\rangle$. These initial and final values are given for the perturbed cluster in Table 4. The maximum expansion in the E and some P models always occurs in the plane of the encounter and is a minimum in the $z$ direction; this last result is consistent with Chandrasekhar's (1942) analysis for the tidal disruption of a star cluster, which shows that disruption is not caused by tidal instability in the $z$ direction. In the fast hyperbolic encounters (H5), the maximum expansions occur in a direction perpendicular to the trajectory of the encounter, which is consistent with the results of RRSDB. In these fast encounters the dynamical friction is more important than the tidal forces, because interpenetration of the clusters occurs, in spite of the short collision times.

**Table 3.** Collision parameters. Columns: (1) model: hyperbolic (H), parabolic (P) and elliptic (E); (2) $N_{part}$, total number of particles of the two clusters; (3) $M_1/M_2$ mass ratio; (4) $e$, eccentricity of the orbit; (5) $p$, pericentre of the orbit; (6) $V_i$, initial relative velocity (km s$^{-1}$).

| Model | $N_{part}$ | $M_1/M_2$ | $r_0$(pc) | $e$ | $p$(pc) | $V_i$ (Km/s) |
|---|---|---|---|---|---|---|
| HAB20 | 20480 | 10 | 70.0 | 5.0 | 20.0 | 11 |
| HAB10 | 20480 | 10 | 70.0 | 5.0 | 10.0 | 14 |
| HAB5 | 20480 | 10 | 70.0 | 5.0 | 5.0 | 19 |
| PAB20 | 20480 | 10 | 70.0 | 1.0 | 20.0 | 4 |
| PAB10 | 20480 | 10 | 70.0 | 1.0 | 10.0 | 4 |
| PAB5 | 20480 | 10 | 70.0 | 1.0 | 5.0 | 4 |
| E9AB10 | 20480 | 10 | 70.0 | 0.9 | 20.0 | 4 |
| HBD20 | 4608 | 10 | 37.0 | 5.0 | 20.0 | 4 |
| HBD10 | 4608 | 10 | 37.0 | 5.0 | 10.0 | 5 |
| HBD5 | 4608 | 10 | 37.0 | 5.0 | 5.0 | 6 |
| PBD20 | 4608 | 10 | 37.0 | 1.0 | 20.0 | 2 |
| PBD10 | 4608 | 10 | 37.0 | 1.0 | 10.0 | 2 |
| PBD5 | 4608 | 10 | 37.0 | 1.0 | 5.0 | 2 |
| E9BD10 | 4608 | 10 | 37.0 | 0.9 | 10.0 | 1 |
| E7BD10 | 4608 | 10 | 37.0 | 0.7 | 10.0 | 1 |
| E6BD10 | 4608 | 10 | 37.0 | 0.6 | 10.0 | 1 |
| HBC20 | 4608 | 10 | 37.0 | 5.0 | 20.0 | 3 |
| HBC10 | 4608 | 10 | 37.0 | 5.0 | 10.0 | 5 |
| HBC5 | 4608 | 10 | 37.0 | 5.0 | 5.0 | 6 |
| PBC20 | 4608 | 10 | 37.0 | 1.0 | 20.0 | 2 |
| PBC10 | 4608 | 10 | 37.0 | 1.0 | 10.0 | 2 |
| PBC5 | 4608 | 10 | 37.0 | 1.0 | 5.0 | 2 |
| E7BC10 | 4608 | 10 | 37.0 | 0.7 | 10.0 | 2 |
| E6BC10 | 4608 | 10 | 37.0 | 0.6 | 10.0 | 1 |
| HCD20 | 1024 | 1 | 20.0 | 5.0 | 20.0 | 2 |
| HCD10 | 1024 | 1 | 20.0 | 5.0 | 10.0 | 2 |
| HCD5 | 1024 | 1 | 20.0 | 5.0 | 5.0 | 3 |
| PCD20 | 1024 | 1 | 20.0 | 1.0 | 20.0 | 1 |
| PCD10 | 1024 | 1 | 20.0 | 1.0 | 10.0 | 1 |
| PCD5 | 1024 | 1 | 20.0 | 1.0 | 5.0 | 1 |
| E7CD5 | 1024 | 1 | 20.0 | 0.7 | 10.0 | 1 |

### 4.4 Comparison of simulations with Magellanic Cloud pairs

Isopleth maps of projected planes at a given time $t$ for a suitable model can be compared with the observed isodensity maps of the Magellanic pairs to infer their dynamics. In Fig. 9 we show time sequences of isopleth maps where the formation of bridges and isophotal twisting in the perturbed cluster occurs for the E, P10 and P20 models. Bridges vanish with increasing eccentricity. In the H models, bridges do not occur, and the perturbed cluster is deformed by dynamical friction mainly in a direction perpendicular to the trajectory of the encounter. The halo expansion survives throughout the $\simeq$90 Myr duration of the present computations, which could be a possible explanation for the existence of some isolated clusters with extended loose outer parts. Several of these evolutionary stages have counterparts in LMC pairs (Fig. 5). For example, the bridge seen in

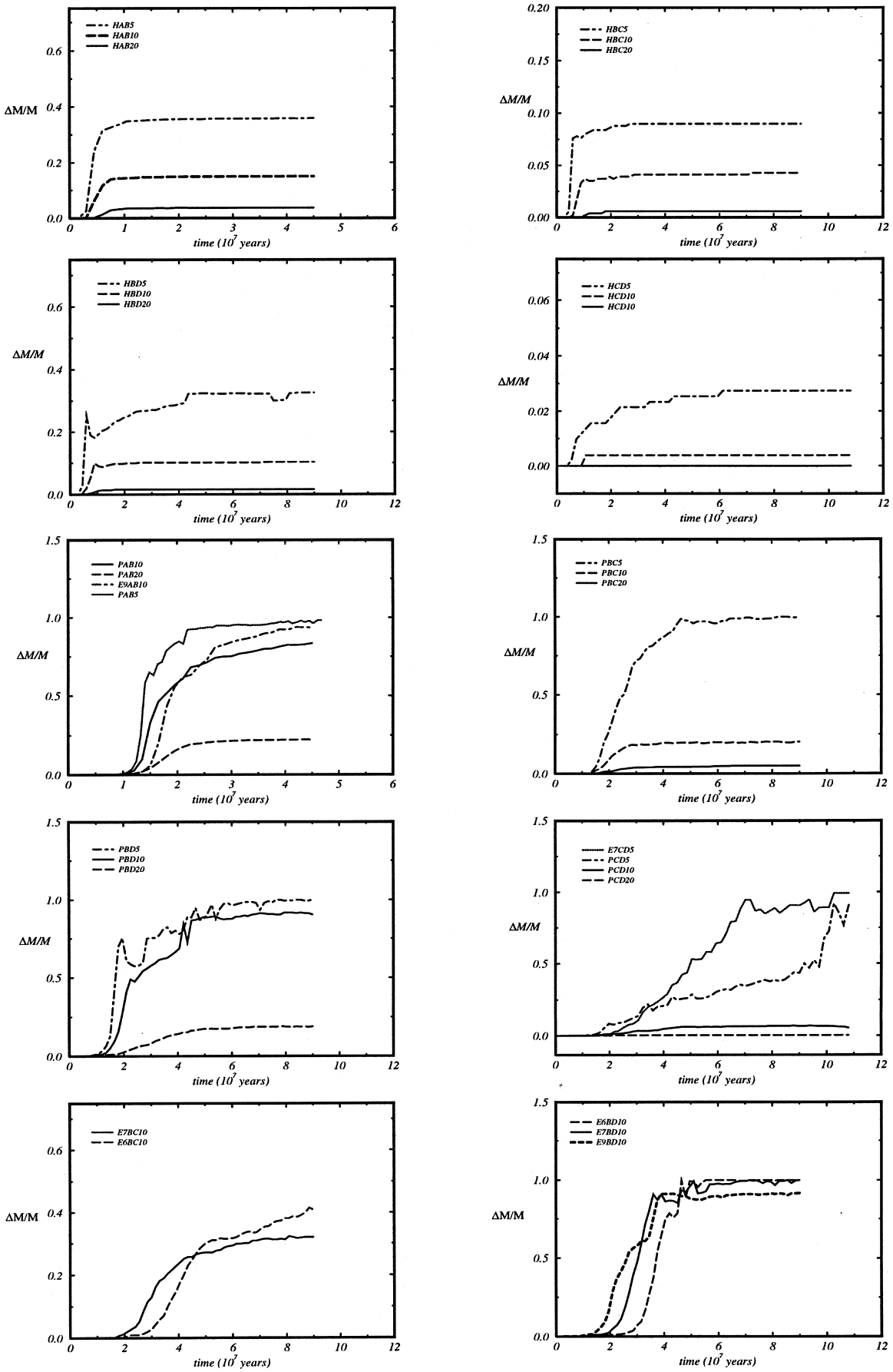


**Figure 7.** Fractional change in mass as a function of time for different models.

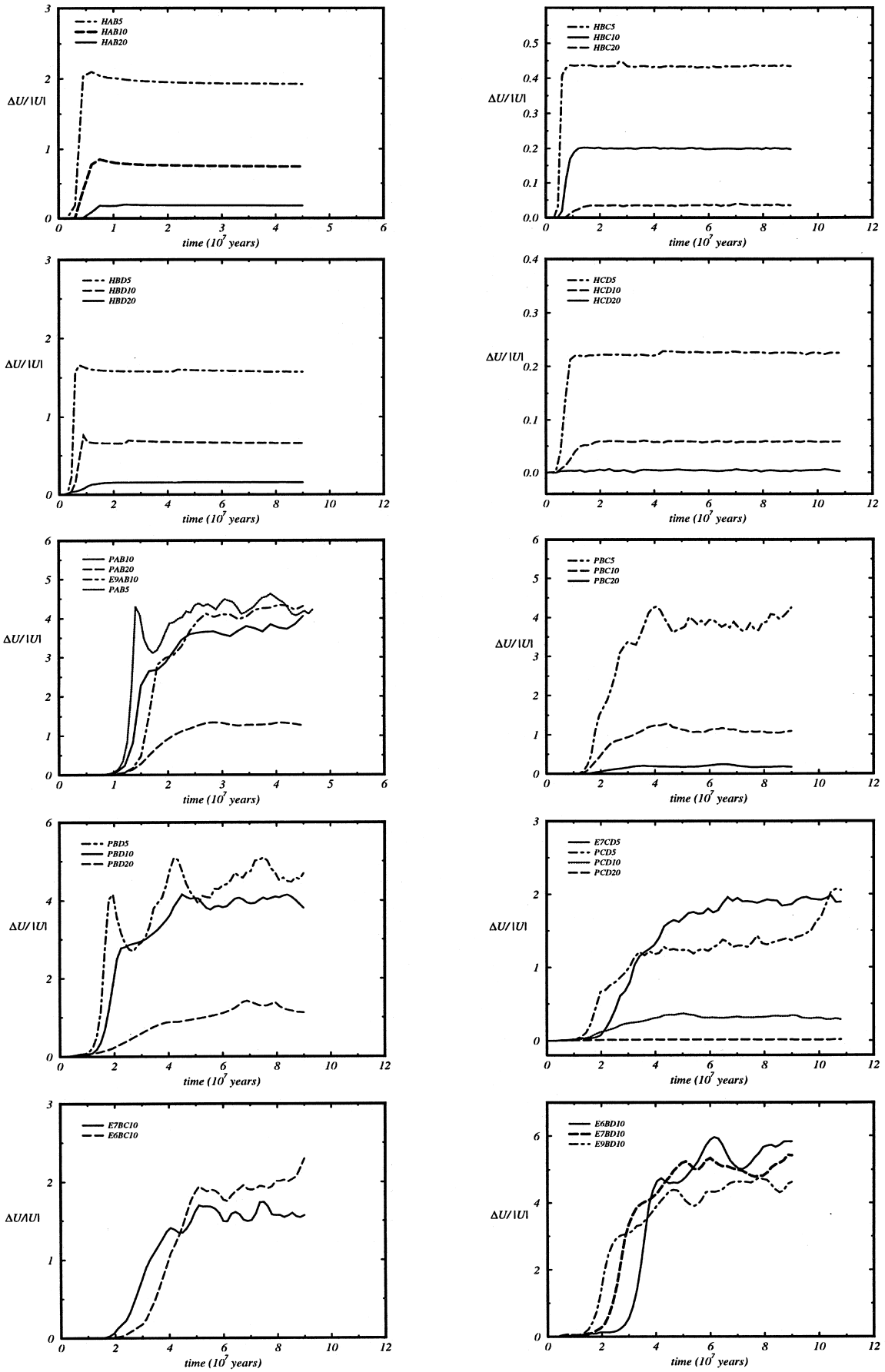


**Figure 8.** Fractional change in energy as a function of time for different models.

**Table 4.** Mass distribution before and after the encounters for the models.

| Model | $<\|X\|>$ | $<\|Y\|>$ | $<\|Z\|>$ |
|---|---|---|---|
| INITIAL | 2.38 | 2.40 | 2.37 |
| HAB20 | 5.16 | 4.57 | 4.46 |
| HAB10 | 11.39 | 13.41 | 14.8 |
| HAB5 | 18.44 | 40.96 | 40.05 |
| PAB20 | 10.32 | 17.78 | 4.42 |
| PAB10 | 20.61 | 42.43 | 9.20 |
| PAB5 | 26.80 | 66.06 | 14.92 |
| E9AB10 | 28.33 | 47.00 | 9.16 |

| Model | $<\|X\|>$ | $<\|Y\|>$ | $<\|Z\|>$ |
|---|---|---|---|
| INITIAL | 2.30 | 2.37 | 2.34 |
| HBD20 | 3.71 | 3.61 | 3.20 |
| HBD10 | 7.10 | 8.69 | 8.73 |
| HBD5 | 13.61 | 23.85 | 21.34 |
| PBD20 | 8.56 | 13.08 | 3.71 |
| PBD10 | 20.61 | 42.11 | 8.34 |
| PBD5 | 18.56 | 48.63 | 12.05 |
| E9BD10 | 20.34 | 41.76 | 7.74 |
| E7BD10 | 23.84 | 28.82 | 6.14 |
| E6BD10 | 24.19 | 18.14 | 5.15 |

| Model | $<\|X\|>$ | $<\|Y\|>$ | $<\|Z\|>$ |
|---|---|---|---|
| INITIAL | 1.30 | 1.32 | 1.28 |
| HBC20 | 1.87 | 1.94 | 1.64 |
| HBC10 | 3.53 | 3.39 | 3.5 |
| HBC5 | 6.01 | 9.06 | 7.31 |
| PBC20 | 3.24 | 4.07 | 1.69 |
| PBC10 | 13.12 | 15.01 | 3.39 |
| PBC5 | 18.7 | 58.05 | 7.62 |
| E7BC10 | 11.5 | 18.78 | 2.85 |
| E6BC10 | 17.36 | 13.60 | 3.15 |

| Model | $<\|X\|>$ | $<\|Y\|>$ | $<\|Z\|>$ |
|---|---|---|---|
| INITIAL | 2.30 | 2.37 | 2.34 |
| HCD20 | 2.44 | 2.28 | 2.36 |
| HCD10 | 4.40 | 4.76 | 4.88 |
| HCD5 | 4.45 | 4.71 | 3.40 |
| PCD20 | 2.65 | 2.35 | 2.32 |
| PCD5 | 9.09 | 20.85 | 6.76 |
| E7CD5 | 10.31 | 9.07 | 4.95 |

the pair NGC 1994/anonymous companion could be associated with the stage of model PAB20 at $t=22.5$ Myr.

In a previous paper, RRSDB have used a similar method to study five pairs in the LMC and found evidence that they are interacting. In the present study we show additional pairs with evidence of interaction when compared with the simulations. Some examples are given in Figs 10, 11 and 12, where we compare models and LMC/SMC cluster pairs using absolute scales in parsecs, and by conveniently rotating models for the best fit to the observations.

The model that best describes the pair NGC 2136/2137 (Fig. 10) is an $XY$ projection of the model (E9AB10) at $t=15$ Myr. Note the similarities, such as a common envelope and the asymmetry in the small cluster halo (NGC 2137). A twisting in the isopleths of the small cluster can also be seen. The model suggests that the cluster NGC 2137 has just passed the pericentre; it is still in physical interaction with NGC 2136 and will probably be disrupted, according to the model evolution. We can also infer that this is a closed-orbit interaction, which suggests that both clusters have a common age. Indeed, NGC 2136/82137 are both blue clusters with similr SWB type (III and II respectively; Bica et al. 1996).

For the pair HS 319/BRHT 52b, the best representation is an $XY$ projection of the model E9AB10 at $t=19.5$ Myr (Fig. 11). Note the similarity of the asymmetry and the isophotal twisting in the small cluster. This suggests that the small cluster is enduring a disruption by dynamical friction.

The pair NGC 294 = L 47/B 67 + BS 63 is best described by an $XY$ projection of the model HBD5 at $t=16.5$ Myr (Fig. 12). Notice the isophotal deformations of the small cluster in the direction perpendicular to the line joining the clusters. This scenario can be explained by a simple projection or by a fast hyperbolic encounter with interpenetration. This kind of encounter basically occurs by capture, which suggests that more probably the clusters have different ages. A colour–magnitude diagram study is necessary to verify this evidence. Notice that the pair described in Bica & Schmitt (1995) is B 67 with BS 63. The present fit suggests that the large neighbour NGC 294 = L 47 might be responsible for the disturbed structure related to B 67 + BS 63.

To test whether simple projection effects could cause the deformation seen in the isodensity maps of cluster pairs, we have overlapped two isolated model clusters and generated isopleth maps for two different lines of sight (Fig. 13): (i) in the left panel the clusters are superimposed in the $XY$ plane; (ii) in the right panel we show the same clusters from an oblique viewing angle. Some isopleth deformations occur from projection effects, but they are minor compared with those arising from interactions (Figs 10 and 11).

## 5 CONCLUSIONS

We have used $N$-body simulations to study the morphology and dynamics of a selection of cluster pairs of the Magellanic Clouds. The main conclusions are as follows.

(i) Disruption of the perturbed cluster (i.e. loss of more than 40 per cent of its mass) occurs mainly if the fractional change of its energy is $\Delta U/|U|>2$.

(ii) Most of the structural changes in the clusters occur after the perturbed cluster passes the closest approach point.

(iii) Cluster pairs involved in the same isophotal envelope, where one of the members presents deformations perpendicular to the line joining the pair, can be the result of an elliptical orbit encounter where the closest approach is $\leq 4.3\,R_{\rm h}$.

(iv) Cluster pairs with isophotal maps linked by bridges, where one of the members presents halo deformations, can be the result of an elliptical/parabolic orbit encounter where the perturbed cluster is disrupting.

(v) Cluster pairs with detached isophotal maps that present deformations perpendicular to the line joining the pair for one member can be the result of a hyperbolic orbit encounter where the closest approach is $\leq 4.3\,R_{\rm h}$.

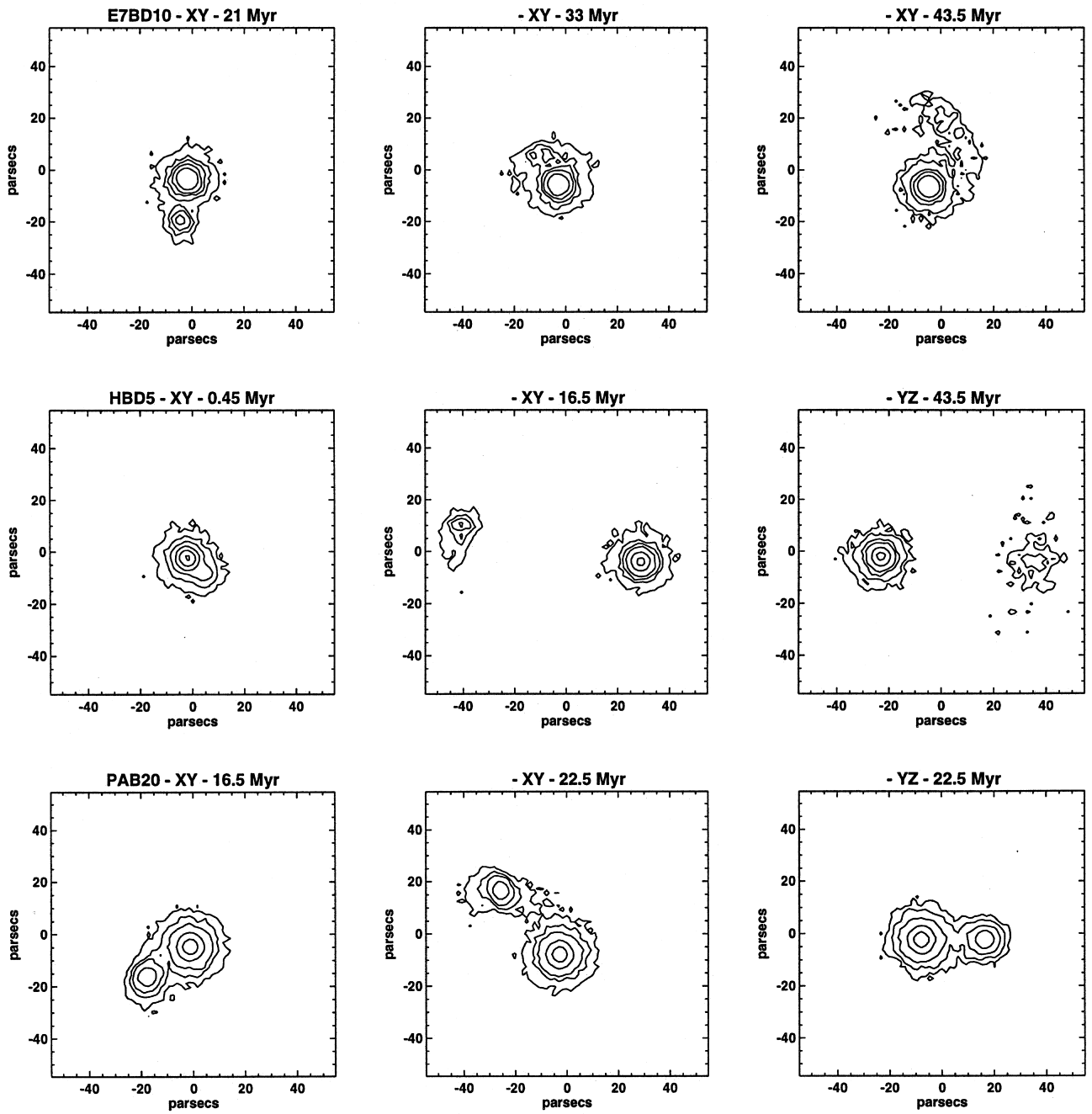


**Figure 9.** Isophotal maps for some sequences of simulations. In each map we indicate the model designation, projected plane and time of the simulation (Myr).

(vi) Isodensity maps of LMC/SMC cluster pairs presented in this paper, when compared with the models, indicate evidence of interaction.

(vii) From the simulations we can estimate that the timescale for a cluster to be disrupted by interaction is not longer than $10^7$ yr. As the available ages for members (Table 2) are in general larger than this value, these clusters survive individually for a considerable time before interacting. This sets a constraint on the smallest distance among the clusters at their formation epoch: $\approx$95 pc for a cluster pair with age 50 Myr, in a closed orbit, increasing to $\approx$400 pc for a 450-Myr pair. Indeed, isophotal distortions occur in general for closed orbit encounters, suggesting a common origin for the clusters, possibly in large complexes sometimes exceeding sizes of 1 kpc, such as some large stellar associations (Lucke & Hodge 1970) or Shapley's constellations (van den Bergh 1981). For clusters in the LMC bar, many pairs occur (Bica et al. 1992), most of them coeval, but some are not. The orbits in such an environment, along the bar, and the high cluster density may favour captures. On the other hand, a cluster pair formation by capture would be an unusual event outside the LMC bar.

The present computations used equal-mass stars, and in future it would be worth exploring the influence of mass segregation in models containing a mass spectrum. In a

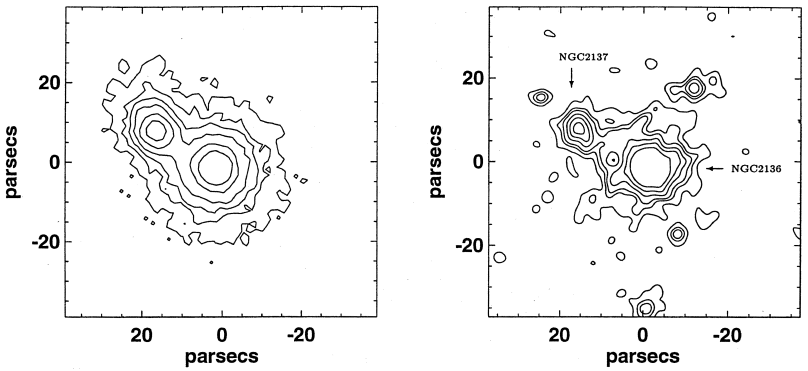


**Figure 10.** Comparison of model E9AB10 (left panel) with the LMC pair NGC 2136/37 (right panel). In this model the projected plane is *XY* and the time of simulation is $t = 15$ Myr.

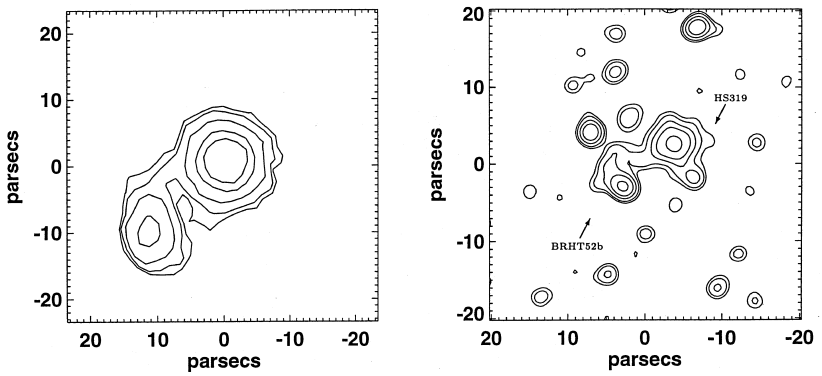


**Figure 11.** Comparison of model E9AB10 (left panel) with the LMC pair HS 319/BRHT 52b (right panel). In this model the projected plane is *XY* and the time of simulations is $t = 19.5$ Myr.

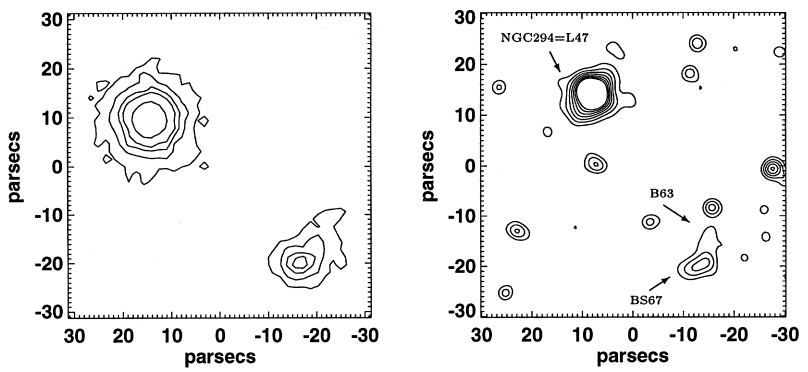


**Figure 12.** Comparison of the model HBD5 (left panel) with the SMC pair NGC 294 = L 47/B 67 + BS 63 (right panel). In this model the projected plane is *XY* and the time of simulation is $t = 16.5$ Myr.

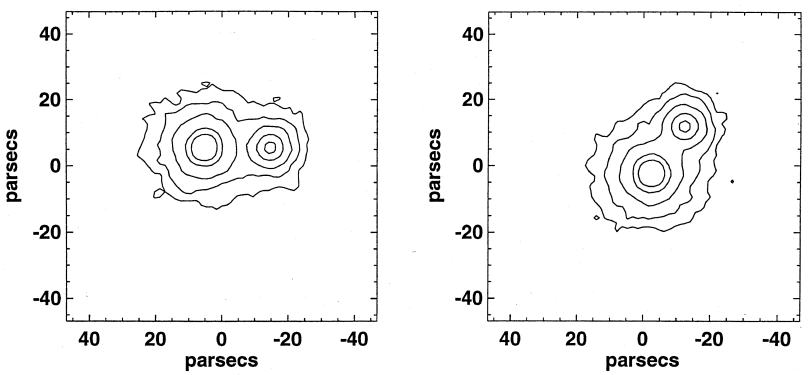


**Figure 13.** Left panel: overlap of isophotal maps for two model clusters, before interacting ($t = 0$), in an *XY* plane projection. Right panel: same clusters from an oblique viewing angle.

multicomponent stellar system, the less massive stars tend to be ejected to the outskirts of the cluster, as a result of particle–particle interactions on a time-scale comparable to the relaxation time (Pryor, Smith & McClure 1986). This suggests that in simulations of interacting cluster pairs including a mass spectrum, the less massive stars would be those producing most of the isophotal distortions.

Photometry of many cluster pairs, both integrated and in the form of colour–magnitude diagrams, is necessary in view of age determination.

The present simulations spanned about 100 Myr and provided evidence of disruption of a small cluster interacting with a massive one, thus suggesting that cluster stars may be ejected to the field by means of this mechanism. The long-term evolution (0.5–1 Gyr) of the present models will give more hints on fundamental questions about galaxy evolution such as (i) the fraction of field stars that might come from clusters disrupted in encounters, and (ii) in the case of mergers/captures, the fraction of stars that is accreted, and how this might change the luminosity function of star clusters in a galaxy. The long-term simulations will be presented in a forthcoming paper, where we shall address these questions.

## ACKNOWLEDGMENTS

We thank Dr Hernquist for allowing us to use TREECODE and the CESUP-UFRGS national supercomputer centre for allotted time on the CRAY YMP-2E computer. We are also grateful to I. Rodrigues for discussions and help in the implementation of several software packages used herein, and to an anonymous referee for interesting remarks. We acknowledge support from the Brazilian Institutions CNPq, CAPES and FINEP.

The images in this study are based on photographic data obtained using the UK Schmidt Telescope, which was operated by the Royal Observatory Edinburgh, with funding from the UK Science and Engineering Council, until 1988 June, and thereafter by the Anglo-Australian Observatory. Original plate material is copyright by the Royal Observatory Edinburgh and the Anglo-Australian Observatory. The plates were processed into the present compressed digital form with their permission. The Digitized Sky Survey was produced at the Space Telescope Science Institute under US Government grant NAG W-2166.

## REFERENCES

Aarseth S. J., Hénon M., Wielen R., 1974, A&A, 37, 183
Aguilar L. A., White S. D. M., 1985, ApJ, 295, 374
Alcaino G., 1978, A&AS, 34, 431
Alladin S. M., 1965, ApJ, 141, 768
Barnes J. E., 1988, ApJ, 331, 699
Barnes J. E., Hut P., 1986, Nat, 324, 446
Barnes J. E., Hut P., 1989, ApJS, 70, 389
Bhatia R. K., Hatzidimitriou D., 1988, MNRAS, 230, 215
Bhatia R. K., MacGillivray H. T., 1988, A&A, 203, L5
Bhatia R. K., MacGillivray H. T., 1989, A&A, 211, 9
Bhatia R. K., Read M. A., Hatzidimitriou D., Tritton S., 1991, A&AS, 87, 335
Bica E., Schmitt H., 1995, ApJS, 54, 33
Bica E., Clariá J. J., Dottori H., 1992, AJ, 103, 1859
Bica E., Clariá J. J., Dottori H., Santos J. F. C., Jr, Piatti A. E., 1996, ApJS, 102, 57
Brück M., 1976, Occas. Rep. R. Obs. Edinb., 1, 1
Chandrasekhar S., 1942, Principles of Stellar Dynamics. Dover, New York
Dekel A., Lecar M., Shaham J., 1980, ApJ, 241, 946
Freeman K. C., Illingworth G., Oemler A., Jr, 1983, ApJ, 272, 488
Hernquist L., 1987, ApJS, 64, 715
Hodge P. W., 1975, Ir. Astron. J., 12, 77
Hodge P. W., Sexton J., 1966, AJ, 71, 363
King I. R., 1966, AJ, 71, 64
Lin D. N. C., Tremaine S., 1983, ApJ, 264, 364
Lindsay E. M., 1958, MNRAS, 118, 172
Lucke P. B., Hodge P. W., 1970, AJ, 75, 171
Miller R. H., 1986, A&A, 167, 41
Namboodiri P. M. S., Kochhar R. K., 1990, MNRAS, 243, 276
Pryor C., Smith G. H., McClure R. D., 1986, AJ, 92, 1358
Rao P. D., Ramamani N., Alladin S. M., 1987, JA&A, 8, 17
Rodrigues I., Rodriguez A., Schmitt H., Dottori H., Bica E., 1994, in Layden A., Smith R. C., Storm J., eds, ESO Conf. Proc. 51, The Local Group: Comparative and Global Properties. ESO-Garching, Garching bei München (RRSDB)
Shapley H., Lindsay E. M., 1963, Ir. Astron. J., 6, 74
van den Bergh S., 1981, A&AS, 46, 79
Westerlund B. E., 1990, A&AR, 2, 29
White S. D. M., 1978, MNRAS, 184, 185